
Article:
Dhimish, Mahmoud, Holmes, Violeta, Mehrdadi, Bruce et al. (2 more authors) (2017) Detecting Defective Bypass Diodes in Photovoltaic Modules using Mamdani Fuzzy Logic System. Global Journal of Researches in Engineering: F Electrical and Electronics Engineering. pp. 33-44. ISSN 0975-5861

Detecting Defective Bypass diodes in Photovoltaic Modules Using Mamdani Fuzzy Logic System

Abstract:

In this paper, the development of fault detection method for PV modules defective bypass diodes is presented. Bypass diodes are nowadays used in PV modules in order to enhance the output power production during partial shading conditions. However, there is lack of scientific research which demonstrates the detection of defective bypass diodes in PV systems. Thus, this paper propose a PV bypass diode fault detection classification based on Mamdani fuzzy logic system, which depends on the analysis of V_{drop}, V_{oc} , and I_{sc} obtained from the I-V curve of the examined PV module.

The fuzzy logic system depends on three inputs, namely percentage of voltage drop (PVD), Percentage of open circuit voltage (POCV), and the percentage of short circuit current (PSCC). The proposed fuzzy system can detect up to 13 different faults associated with defective and non-defective bypass diodes. In addition, the proposed system was evaluated using two different PV modules under various defective bypass conditions. Finally, in order to investigate the variations of the PV module temperature during defective bypass diodes and partial shading conditions, i5 FLIR thermal camera was used.

1. Introduction:

As prices in the photovoltaic (PV) industry have decreased considerably in the last few years, reliability questions have been proportional increased interest. The performance and efficiency of PV modules are affected by several factor such as solar irradiance, ambient temperature, humidity, and wind [1-3]. In addition, several work have studied and evaluated the performance of PV modules under different climate conditions, in particular the effect of sand dust accumulation and partial shading on the output power of PV modules and PV arrays [4 & 5].

In addition, PV modules output power performance could be decreased due to the PV cracks [6 & 7]. As reported in [8], PV cracks occur in PV solar cells due to partial shading conditions affecting some solar cells while the rest are under normal operation mode, also it might occur due to the dust and hot spots in PV modules. To solve this problem in PV modules, a bypass diodes connection to the PV strings is recommended.

As a result of these factors impacting the PV performance, a fault detection methods is indeed important to be employed and further investigate in PV systems. In general, fault detection method in PV systems can be grouped as visual (discoloration, surface soiling, and delamination), thermal (hot spots and PV micro cracks), and electrical (I-V, and P-V curve analysis, and transmittance line diagnosis) [9 & 10]. In this paper, we focus on an electrical method. Multiple PV fault detection based electrical methods for PV system are based on:

1. Methods do not require climate data (such as solar irradiance and PV module temperature). In [11] the authors developed a method based on the Earth Capacitance Measurements (ECM) to detect the disconnection of a PV module. The first Time-Domain Reflectometry (TDR) technique was proposed by [12]. This technique is used to detect the disconnection of PV strings as well as the impedance change due to PV degradation. Finally, [13-15] proposed a statistical analysis PV fault detection method based on t-test and standard deviation, which can be used to detect PV failure, and faults associated with maximum power point tracking (MPPT) units.
2. Methods based on the analysis of the current-voltage I-V characteristics. In [16], the analysis of the I-V and P-V curve was used to investigate the performance of the PV module, thus, detecting possible faults such as partial shading and faulty PV strings. In [17 & 18], the authors calculate the fill factor (FF), series resistance (R_s), and the shunt resistance (R_{sh}) from the I-V curve to investigate the performance of multiple PV configuration systems.
3. Methods based on artificial intelligence (AI) techniques. In [19 & 20] the authors proposed a PV fault detection algorithm which can

identify the partial shading conditions in PV modules based on a fuzzy logic system. However, the proposed technique cannot identify the impact of bypass diodes in PV modules, which has been investigated by [21 & 22]. In addition, a learning method based on Expert Systems is developed by [23-25] to identify faults in PV modules due to partial shading and inverter's failure. Furthermore, in [26], an artificial neural network (ANN) is used in order to classify different types of faults occurring in a PV array. In this case, the ANN takes as inputs the current and the voltage at maximum power point, and the temperature of the PV module. Different methods based on the Takagie Sugeno Kahn Fuzzy Rule (TSKFRBS) have been described in [27 & 28].

The main contribution of this work is to present a new PV fault detection method based on Mamdani fuzzy logic system, which can detects the defective bypass diodes and partial shading conditions. The fuzzy logic system depends on three inputs:

1. Percentage of voltage drop (PVD)
2. Percentage of open circuit voltage (POCV)
3. Percentage of short circuit current (PSCC)

Finally, in order to investigate the variations of the PV module temperature during defective bypass diodes and partial shading conditions, i5 FLIR thermal camera was used. Several test have been carried out using two diffident PV modules with nominal peak power 220 W_p and 130 W_p.

2. Examined PV module characteristics:

The PV system used in this work comprises a PV plant containing 9 polycrystalline silicon PV modules each with a nominal power of 220 Wp. The photovoltaic modules are organized in 3 strings and each string is made up of 3 series-connected PV modules. Using a photovoltaic connection unit which is used to enable or disable the connected of any PV modules from the entire GCPV plant, each photovoltaic string is connected to a Maximum Power Point Tracker (MPPT) which has an output efficiency not less than 98.5% [29]. The existing PV system is shown in Figure 1a.

The SMT6 (60) P solar module manufactured by Romag has been used in this work. The tilt angle of the PV installation is 42°. The electrical characteristics of the solar module are shown in Table 1. Additionally, the standard test condition (STC) for these solar panels are: solar irradiance (G): 1000 W/m^2 and module temperature (T): 25 °C.

Each examined PV module comprises three bypass diodes which are connected in parallel to each PV string. Figure 1b shows the connection of the bypass diodes, where Figure 2c shows the junction box placed at the back of the PV modules.

Table 1 Examined PV electrical characteristics

PV module electrical characteristics	Value
Power at maximum power point (P_{mpp})	220 W
Voltage at maximum power point (V_{mpp})	28.7 V
Current at maximum power point (I_{mpp})	7.67 A
Open Circuit Voltage (V_{oc})	36.74 V
Short Circuit Current (I_{sc})	8.24 A
Number of cells connected in series	60
Number of cells connected in parallel	1

3. Inspection and validation method:

In this work, the MPPT units were used to measure the voltage, and current using the internal sensors embedded with this device. Subsequently, the MPPT units are connected to a Virtual instrumentation (VI) LabVIEW software in order to simulate the current-voltage (I-V) curve of the examined PV modules.

Furthermore, the investigation of the temperature variations during partial shading and faulty bypass diodes (bypass diode disconnected from the PV modules) have been captured using i5 FLIR thermal camera. This camera has the following specification:

- Thermal image quality: 100x100 pixels
- Field of view: 21^0 (H) x 21^0 (V)
- Thermal sensitivity: 32.18 F

(a)

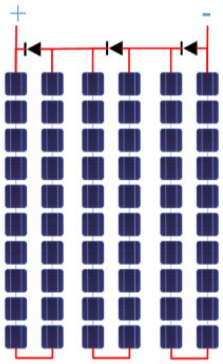

(b)

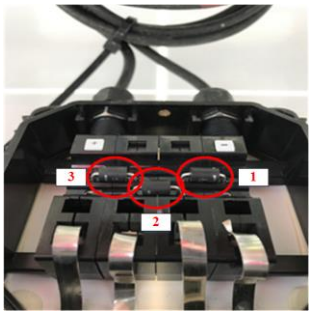

(c)

Fig 1: (a) Examined PV system installed at the University of Huddersfield, United Kingdom, (b) Internal bypass connection for each PV module, (c) Junction box placed at the back of the PV modules

Experimental results:

In this section, the behavior of the examined PV modules under various partial shading conditions and faulty bypass diodes will be presented.

1. I-V curve characteristics under partial shading conditions:

The first test will demonstrate the impact of partial shading conditions on the I-V curve for a standalone PV module. The first PV module in the PV system will be coved by an opaque object to examine the PV module under various partial shading conditions as shown in Figure 3a.

Multiple experiments have been conducted under various partial shading conditions, starting from 10% and ending up with 90%. Three thermal images of the examined PV module under partial shading conditions (10%, 30%, and 60%) are shown in Figure 3. In addition, all experiments were performed while there is no defective bypass diodes connected in the tested PV module.

Figure 2a and Figure 2b show the experiment output for the I-V and P-V curves for all tested shading conditions. As can be noticed, while increasing the percentage of shading the V_{oc} of the PV module decrease. However, the I_{sc} remains the same at 8.18 A.

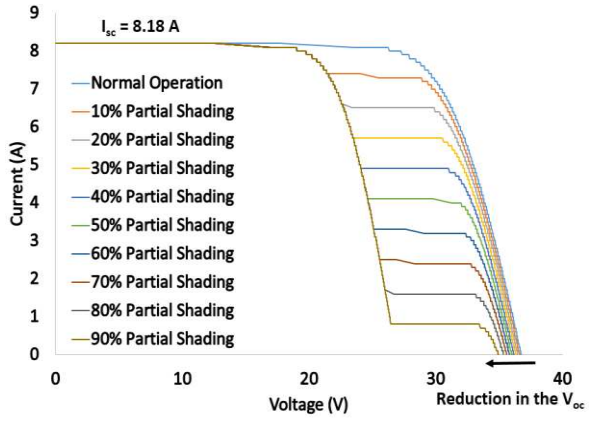

(a)

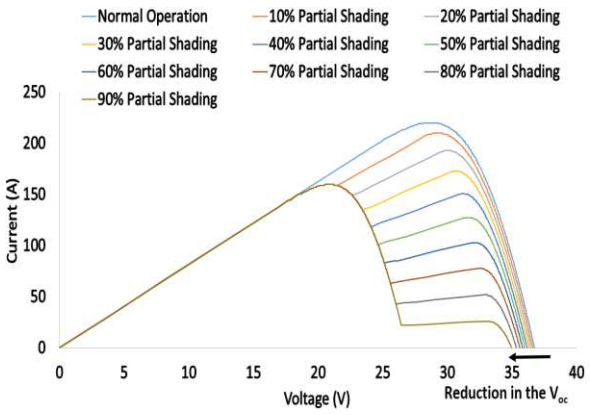

(b)

Fig 2: (a) I-V curve characteristics under various partial shading conditions affecting the PV module, (b) P-V curve characteristics under various partial shading conditions affecting the PV module

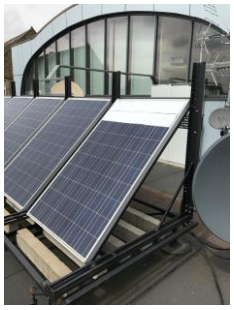

(a)

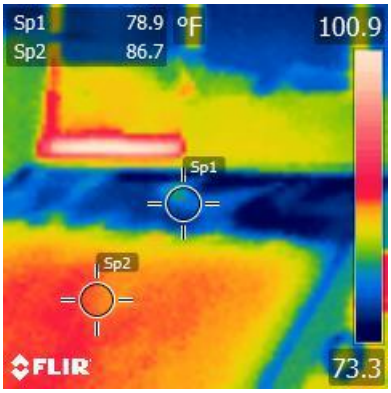

(b)

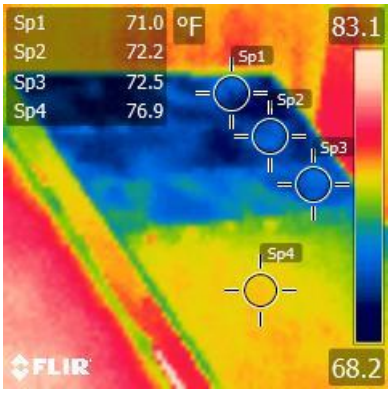

(c)

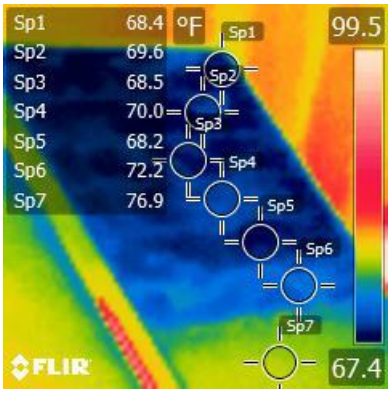

(d)

Fig 3: (a) Real image of the examined PV module coved by opaque object, (b) 10% partial shading, (c) 30% partial shading, (d) 60% partial shading

2. *I-V curve characteristics under 20% partial shading condition and faulty bypass diodes:*

This test was experimentally evaluated while disconnecting one, two, and three bypass diodes in the PV module under 90% partial shading condition (worst case scenario).

As shown in Figure 4a, during 90% partial shading and no disconnection of PV module bypass diodes, PV module I-V curve started to drop its I_{sc} at 18 V, we called this scenario the V_{drop} in the I-V curve. However, the first drop in the I-V curve while disconnecting one bypass diode is at 16 V. Faster drop is associated with 90% partial shading and 2 faulty bypass diodes in the PV module.

The last case, when all PV module bypass diodes completely removed during 90% partial shading condition. In this case, the drop in the I_{sc} is obtained at the start of the I-V curve (at 0 V). This loss in the current will affect the output power of the PV module significantly. The output power obtained in each case scenario can be presented as follows:

- No fault in the bypass diodes:
  - P_{mpp} = 159.8 W
- Disconnecting 1 bypass diode:
  - P_{mpp} = 141.5 W
- Disconnecting 2 bypass didoes:
  - P_{mpp} = 104.8 W
- Disconnecting all bypass didoes:
  - P_{mpp} = 18.84 W

While disconnection bypass diodes from the PV module during partial shading conditions, the PV module output power will decrease. This phenomenon occur due to the impact of the reverse-bias feature of the bypass diodes. In addition, Figure 4b shows that while disconnecting a bypass diode, the temperature raises in the PV string associated with the faulty bypass diode location. The increase of the PV sting temperature will decrease the PV output power. According to Figure 4b, the increase of the PV string temperature is equal to:

66.2 (PV string without bypass diode) – 62.9 (adjacent PV strings with bypass diodes) = 3.3 F

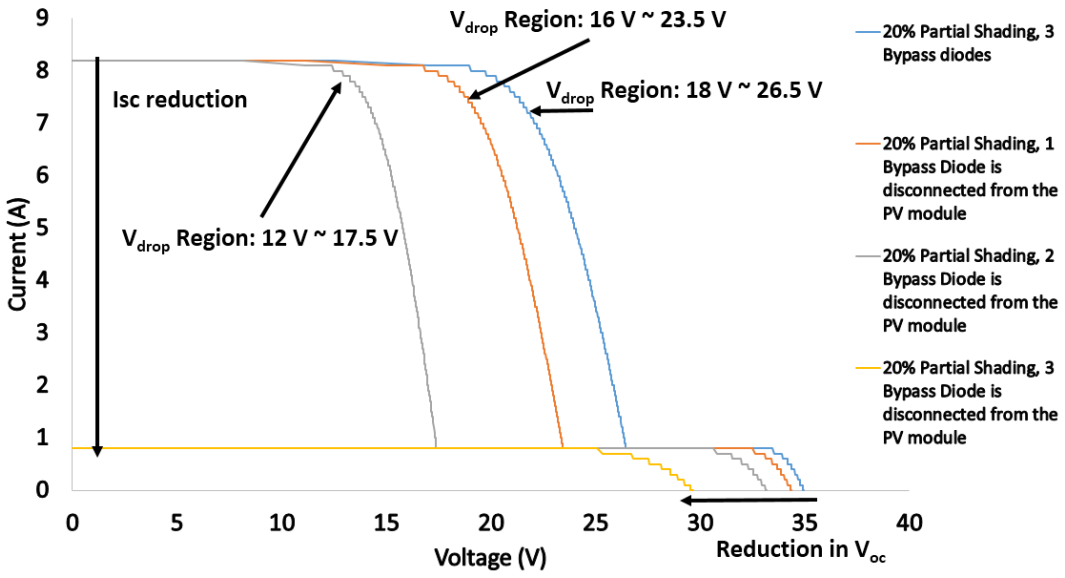

(a)

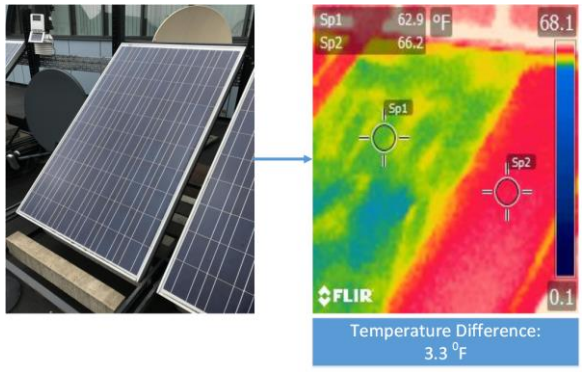

(b)

Fig 4: (a) I-V curves under various conditions affecting the examined PV module, (b) Real image and thermography image of the examined PV module while disconnecting one bypass diode from the first PV string

Since the voltage drop (V_{drop}) has been measured during worst case scenario at each I_{sc} level of the examined I-V curves, it has been found that the V_{drop} in each examined case can be classified as the following:

- No fault in the bypass diodes:
  - V_{drop} Region: 18 ~ 26.5 V
- Disconnecting 1 bypass diode:
  - V_{drop} Region: 16 ~ 23.5 V
- Disconnecting 2 bypass didoes:
  - V_{drop} Region: 12 ~ 17.5 V
- Disconnecting all bypass didoes:
  - V_{drop} Region: 0 ~ 2.87 V

In order to generalize the findings of the V_{drop}, the percentage of V_{mpp} has been compared with the V_{drop} values, which can be formalized as stated in Eq. (1) by the voltage drop percentage (PVD).

$$\text{Percentage of Voltage Drop (PVD)} = \frac{V_{drop}}{V_{mpp}} \times 100 \quad (1)$$

The following calculations show the percentage of voltage drop based on (1) which is validated using the examined I-V curve shown in Figure 4a.

No fault in the bypass diodes:

$$\text{PVD} = \frac{17.5 \sim 26.5}{28.7} \times 100 = 61.0\% \sim 92.3\%$$

Disconnecting 1 bypass diode:

$$\text{PVD} = \frac{15 \sim 23.5}{28.7} \times 100 = 52.2\% \sim 81.9\%$$

Disconnecting 2 bypass didoes:

$$\text{PVD} = \frac{10.5 \sim 17.5}{28.7} \times 100 = 36.5\% \sim 61\%$$

Disconnecting all bypass didoes:

$$\text{PVD} = \frac{0 \sim 2.87}{28.7} \times 100 = 0\% \sim 10\%$$

As can be noticed, the regions of the PVD are overlapping, and in order to increase the detection accuracy of the bypass diodes regions, the percentage of open circuit voltage (POCV) is used. The POCV is calculated using (2).

$$\text{Percentage of open circuit voltage} = \frac{\text{Measured Voc}}{\text{Theoretical Voc}} \times 100 \quad (2)$$

From the results obtained previously in Figure 4a, the POVC for each tested case scenario has been calculated as the following:

No fault in the bypass diodes:

$$\text{POVC} = \frac{36.74 \sim 35}{36.74} \times 100 = 100\% \sim 95.3\%$$

Disconnecting 1 bypass diode:

$$\text{POVC} = \frac{36.74 \sim 33.5}{36.74} \times 100 = 100\% \sim 91.2\%$$

Disconnecting 2 bypass didoes:

$$\text{POVC} = \frac{36.74 \sim 32.1}{36.74} \times 100 = 100\% \sim 87.3\%$$

It is also worthy to mention the behavior of the I-V curves based on the measured I_{sc} for each examined case. Since I_{sc} is another variable which could be used to examine the faulty bypass diodes in PV modules. For that reason, percentage of short circuit current drop (PSCC) has been used and presented by Eq. (3).

$$\text{Percentage of Short Circuit Current} = \frac{\text{Measured Isc}}{\text{Theoretical Isc}} \times 100 \quad (3)$$

The PSCC is equal to 1 in the first 3 cases (no fault in the bypass diodes, disconnecting 1 bypass diode, and disconnecting 2 bypass diodes). However, the PSCC was evaluated using partial shading conditions between 0% up to 90% while disconnecting all bypass diodes in the examined PV module. The PSCC results are shown in Table 2, where the I-V curve simulation is presented in Fig. 5.

The result shows that the percentage of PSCC depends on the percentage of shading affecting the PV module. An increase of the partial shading results a decrease in the PSCC percentage.

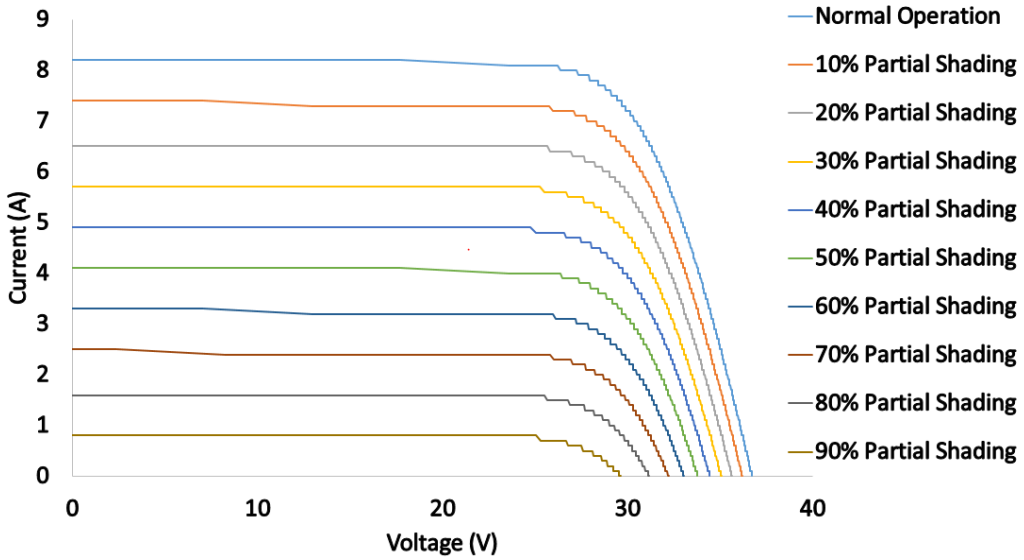

Fig 5: I-V curve simulation under various partial shading conditions while disconnecting all bypass diodes from the examined PV module.

Table 2 PSCC Results for an Examined PV module while disconnecting all bypass diodes

Shading Percentage %	Measured I_{sc} (A)	PSCC %
Normal Operation	8.18	100
10%	7.37	90
20%	6.55	80
30%	5.73	70
40%	4.91	60
50%	4.09	50
60%	3.28	40
70%	2.46	30
80%	1.64	20
90%	820 mA	10

3. ***Proposed fault detection system:***

In this section, the proposed PV bypass diode fault detection system will be presented. First of all, the fault detection system proposed in this paper is capable of detecting faults associated with bypass diodes and partial shading conditions affecting the PV modules.

The detection system is based on the variations of the I-V curve V_{drop}, I-V curve V_{oc}, and I-V curve I_{sc}. Next, Mamdani fuzzy logic system is used to detect the faults in the examined PV module. Subsequently, the fuzzy system is based on three inputs:

1. PVD
2. POVC
3. PSCC

All inputs are processed by the fuzzy logic system based on the membership functions shown in Figure 7a, where all the percentages are discussed previously in section 2.

The output of the fuzzy logic system can classify 13 different type of fault associated with PV bypass diodes and partial shading conditions. Furthermore, Figure 7b illustrates the output membership function used in the fuzzy system. In addition, the list of the faults are shown in Figure 7c.

The fuzzy logic system rule are based on: if, and statement. All selected rules in the fuzzy logic is presented in Appendix A.

The main question related to the structure of the fuzzy logic system, that if the rules and classification could be used in other PV modules? - The answer will be briefly answered next section, however, as can be seen in Figure. 6, the PVD, POCV and PSCC depends on the ratio of the measured and theoretical PV parameters, thus, these ratios are fixed through any tested PV module. As a result of that, the fuzzy logic could be used to classify the faulty bypass diodes in other PV modules as appropriate.

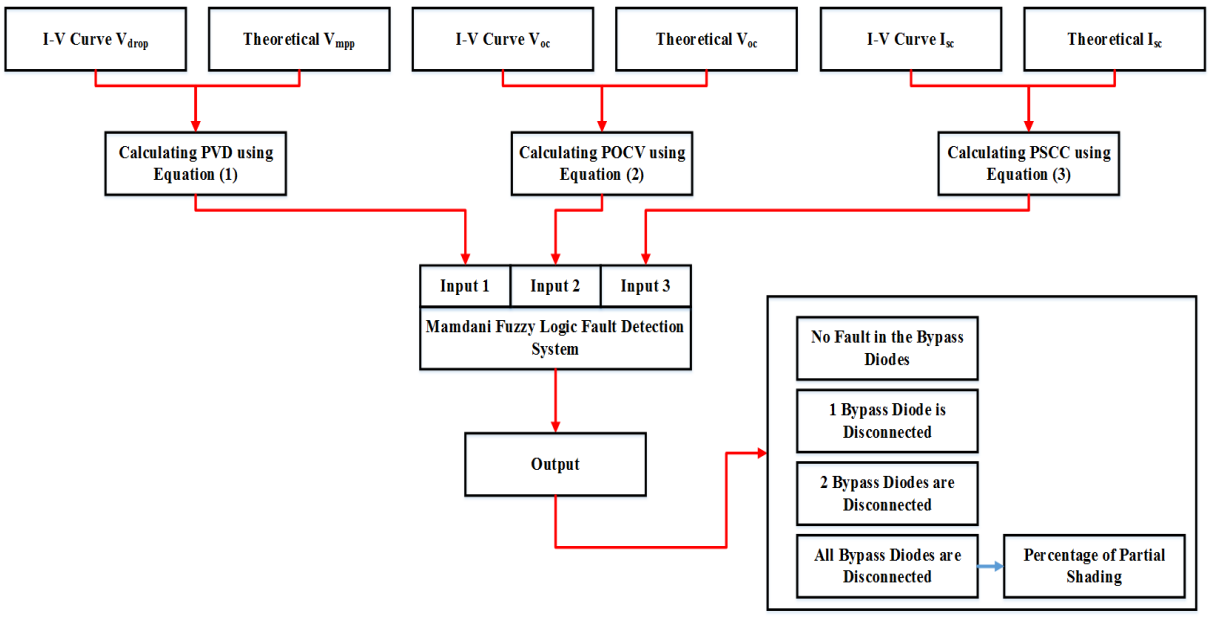

Fig 6: Proposed fault detection system using Mamdani fuzzy logic system

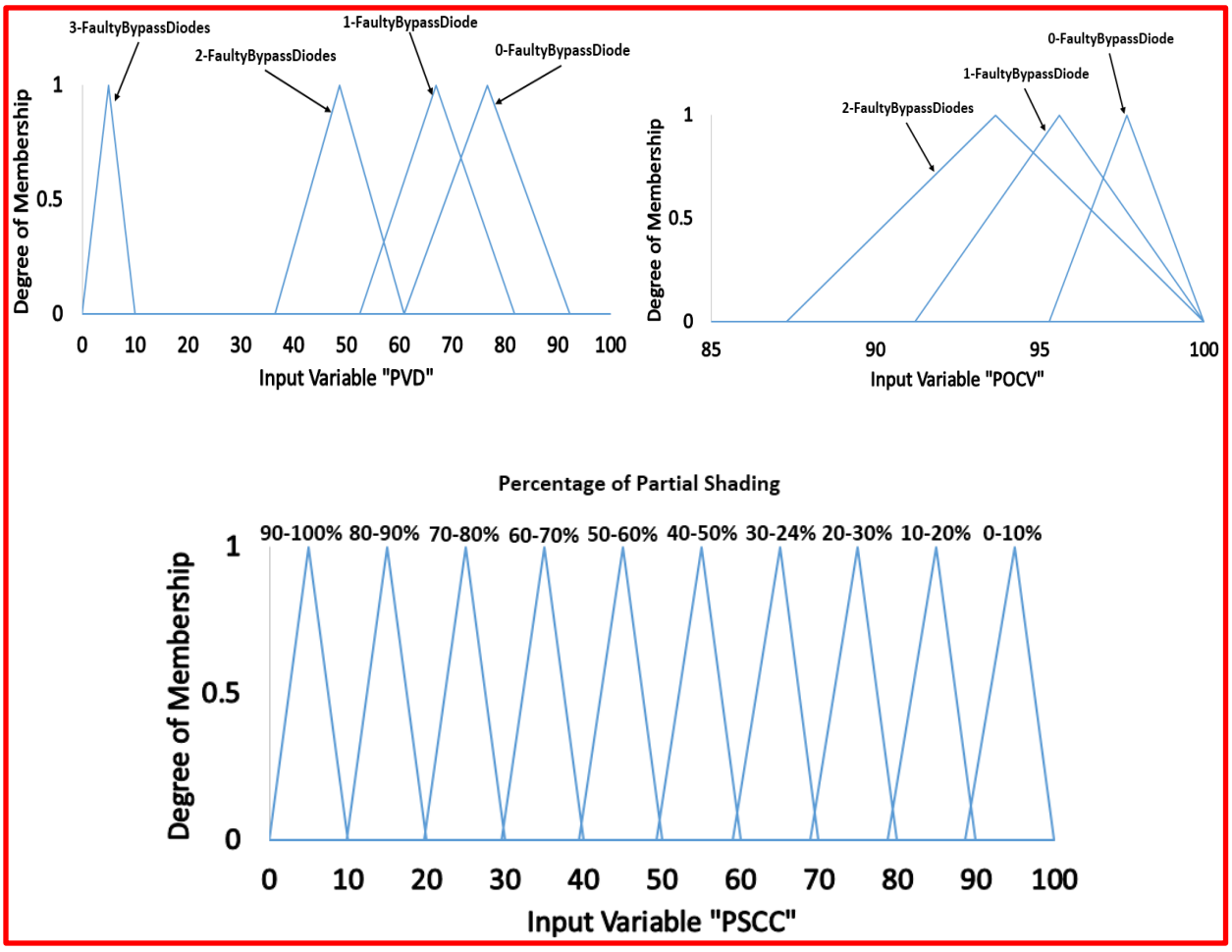

(a)

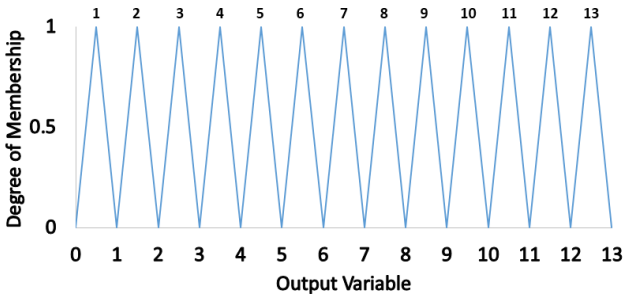

(b)

1 >> No Faults in the Bypass Diodes
2 >> 1 Fualty Bypass Diode
3 >> 2 Faulty Bypass Diodes
4 >> 3 Faulty Bypass Diodes & 0-10% Partial Shading
5 >> 3 Faulty Bypass Diodes & 10-20% Partial Shading
6 >> 3 Faulty Bypass Diodes & 20-30% Partial Shading
7 >> 3 Faulty Bypass Diodes & 30-40% Partial Shading
8 >> 3 Faulty Bypass Diodes & 40-50% Partial Shading
9 >> 3 Faulty Bypass Diodes & 50-60% Partial Shading
10 >> 3 Faulty Bypass Diodes & 60-70% Partial Shading
11 >> 3 Faulty Bypass Diodes & 70-80% Partial Shading
12 >> 3 Faulty Bypass Diodes & 80-90% Partial Shading
13 >> 3 Faulty Bypass Diodes & 90-100% Partial Shading

(c)

Fig 7: (a) Input variables for the proposed fuzzy logic fault detection system, (b) output variable for the fuzzy logic fault detection systems, (c) List of faults which can be detected using the fuzzy logic system

4. *Validation of the proposed fault detection system using KC130GHT PV module:*

In this section, the proposed fault detection system will be evaluated using a different PV module installed at the University of Huddersfield, where the electrical characteristics of the PV module is shown in Table 3. Real image of the PV module is shown in Figure 7. Additionally, the PV strings are connected to three bypass diodes.

In this section, two case scenarios will be evaluated, the first case is when the PV module under one defective bypass diode, where the second case where the PV module under three defective bypass diodes.

Table 3 KC130GHT PV module electrical characteristics

PV module electrical characteristics	Value
Power at maximum power point (P_{mpp})	130 W
Voltage at maximum power point (V_{mpp})	17.6 V
Current at maximum power point (I_{mpp})	7.39 A
Open Circuit Voltage (V_{oc})	21.9 V
Short Circuit Current (I_{sc})	8.02 A
Number of cells connected in series	36
Number of cells connected in parallel	1

Fig 8: Real image of KC130GHT PV module

1. PV module under one defective bypass diode and 35% partial shading:

This test was evaluated when the PV module has one defective bypass diode. The PV module output parameters: V_{drop}, V_{oc}, and I_{sc} are shown in Figure 9a.

The percentages PVD, POVC, PSCC are equal to 58.52%, 99.08% and 100%. Next, these percentages are processed by the fuzzy logic system.

As shown in Figure 9a, the output of the fuzzy system is equal to 1.91, which is between the region "1-2". This region indicates that there is one defective bypass diode in the PV module. In addition, the classifications of all regions are previously described in Figure 7c.

In conclusion, this test was performed by the fuzzy logic, and it has successfully detected the defective bypass diode in the PV module.

2. PV module under three defective bypass diodes and 65% partial shading:

The second test, was performed when the PV module has three defective bypass diodes (all bypass diodes has been removed) and this test was evaluated while covering 65% of the PV module using an opaque paper.

The output performance of the PV module parameters is shown in Figure 9b. The theoretical I_{sc} dropped down to 2.81A after 0.3V. The percentage as PVD, POVC and PSCC are equal to 1.70%, 91.32%, and 35.04%.

The output of the fuzzy system is equal to 9.5, which is between the regions "9-10". This region indicates that there is 3 faulty bypass diodes and 60-70% partial shading affects the PV module.

Both tests indicate that the proposed detection system is capable of detecting the defective bypass diodes in the PV module. Subsequently, there is a high accuracy in the fuzzy logic system output results comparing to the faulty conditions affecting the examined PV module.

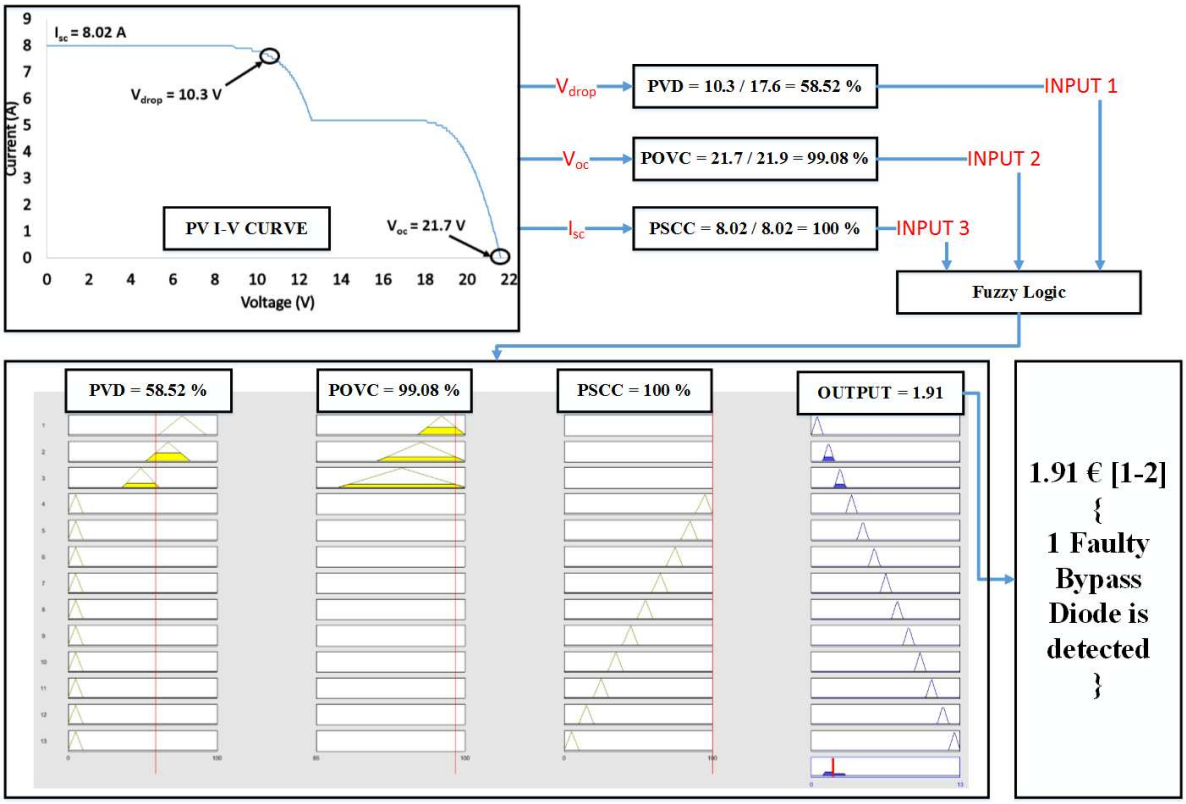

(a)

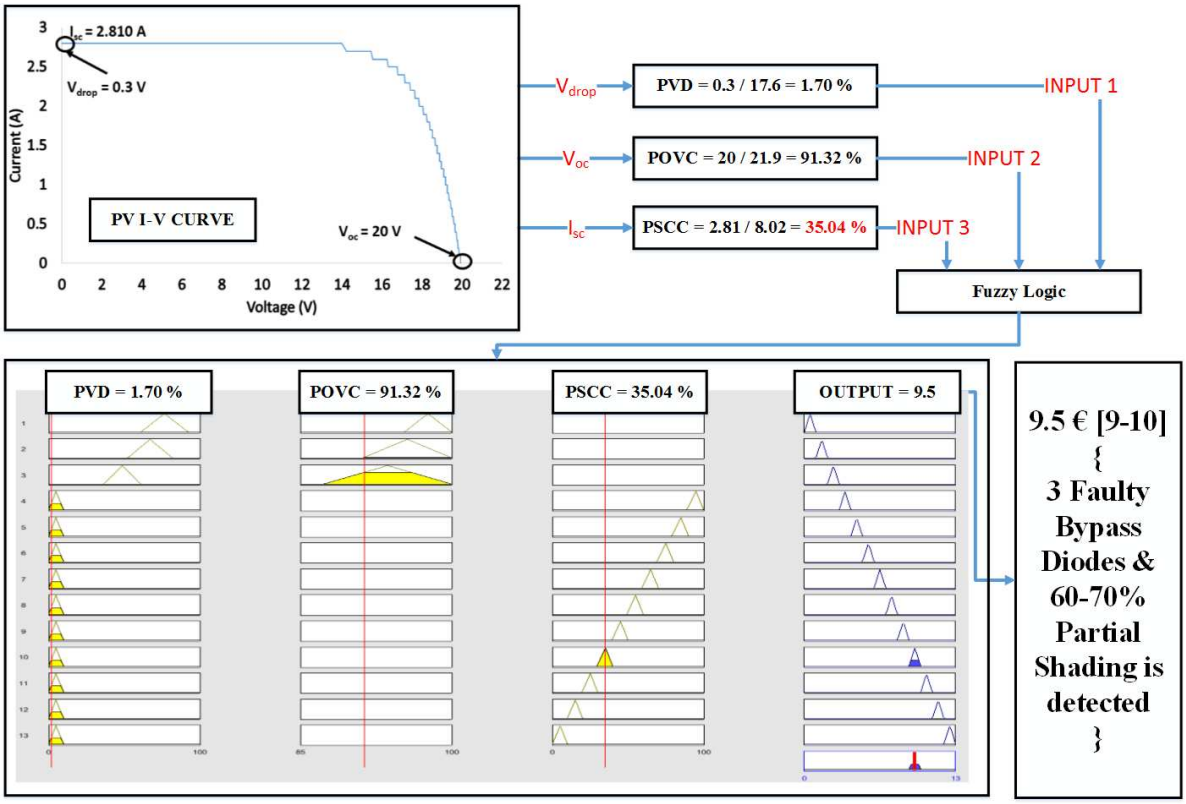

(b)

Fig 9: (a) Output results for 1 faulty bypass diode "case senario1", (b) Output results for 3 faulty bypass diodes & 60-70% partial shading "case scenario 2"

5. Conclusion:

This paper proposed a fault detection method for PV module defective bypass diodes. The detection method is based on Mamdani fuzzy logic system, which depends on the analysis of V_{drop}, V_{oc}, and I_{sc} obtained from the I-V curve of the examined PV module.

The fuzzy logic system depends on three inputs, namely percentage of voltage drop (PVD), Percentage of open circuit voltage (POCV), and the percentage of short circuit current (PSCC). The proposed fuzzy system can detect up to 13 different faults associated with defective and non-defective bypass diodes.

The detection system achieved high detection accuracy during the validation process. In addition, the fuzzy system was evaluated using two different PV modules installed at the University of Huddersfield. Finally, in order to investigate the variations of the PV module temperature during defective bypass diodes and partial shading conditions, i5 FLIR thermal camera was used.

In future, it is intended to extend the present work to detect the faults in PV bypass diodes using the analysis of the series resistance (R_s) and shunt resistance (R_{sh}) of the PV module. In addition, the fuzzy system could be replaced with artificial neural network (ANN).

6. References:

[1] Kaldellis, J. K., Kapsali, M., & Kavadias, K. A. (2014). Temperature and wind speed impact on the efficiency of PV installations. Experience obtained from outdoor measurements in Greece. *Renewable Energy*, *66*, 612-624.

[2] Eke, R., & Betts, T. R. (2017). Spectral irradiance effects on the outdoor performance of photovoltaic modules. *Renewable and Sustainable Energy Reviews*, *69*, 429-434.

[3] Dhimish, M., & Holmes, V. (2016). Fault detection algorithm for grid-connected photovoltaic plants. *Solar Energy*, *137*, 236-245.

[4] Saidan, M., Albaali, A. G., Alasis, E., & Kaldellis, J. K. (2016). Experimental study on the effect of dust deposition on solar photovoltaic panels in desert environment. *Renewable Energy*, *92*, 499-505.

[5] Ramli, M. A., Prasetyono, E., Wicaksana, R. W., Windarko, N. A., Sedraoui, K., & Al-Turki, Y. A. (2016). On the investigation of photovoltaic output power reduction due to dust accumulation and weather conditions. *Renewable Energy*, *99*, 836-844.

[6] Dhimish, M., Holmes, V., Mehrdadi, B., & Dales, M. (2017). The Impact of Cracks on Photovoltaic Power Performance. *Journal of Science: Advanced Materials and Devices*.

[7] Dolara, A., Lazaroiu, G. C., Leva, S., Manzolini, G., & Votta, L. (2016). Snail trails and cell microcrack impact on PV module maximum power and energy production. *IEEE Journal of Photovoltaics*, *6*(5), 1269-1277.

[8] Dhimish, M., Holmes, V., Dales, M., & Mehrdadi, B. (2017). The effect of micro cracks on photovoltaic output power: case study based on real time long term data measurements. *Micro & Nano Letters*.

[9] Alam, M. K., Khan, F., Johnson, J., & Flicker, J. (2015). A comprehensive review of catastrophic faults in PV arrays: types, detection, and mitigation techniques. *IEEE Journal of Photovoltaics*, *5*(3), 982-997.

[10] Tsanakas, J. A., Ha, L., & Buerhop, C. (2016). Faults and infrared thermographic diagnosis in operating c-Si photovoltaic modules: A review of research and future challenges. *Renewable and Sustainable Energy Reviews*, *62*, 695-709.

[11] Takashima, T., Yamaguchi, J., Otani, K., Oozeki, T., Kato, K., & Ishida, M. (2009). Experimental studies of fault location in PV module strings. *Solar Energy Materials and Solar Cells*, *93*(6), 1079-1082.

[12] Schirone, L., Califano, F. P., & Pastena, M. (1994). Fault detection in a photovoltaic plant by time domain reflectometry. *Progress in Photovoltaics: Research and Applications*, *2*(1), 35-44.

[13] Dhimish, M., Holmes, V., & Dales, M. (2017). Parallel fault detection algorithm for grid-connected photovoltaic plants. *Renewable Energy*, *113*, 94-111.

[14] Silvestre, S., da Silva, M. A., Chouder, A., Guasch, D., & Karatepe, E. (2014). New procedure for fault detection in grid connected PV systems based on the evaluation of current and voltage indicators. *Energy Conversion and Management*, *86*, 241-249.

[15] Vergura, S., Acciani, G., Amoruso, V., Patrono, G. E., & Vacca, F. (2009). Descriptive and inferential statistics for supervising and monitoring the operation of PV plants. *IEEE Transactions on Industrial Electronics*, *56*(11), 4456-4464.

[16] Miwa, M., Yamanaka, S., Kawamura, H., & Ohno, H. (2006, May). Diagnosis of a power output lowering of PV array with a (-dI/dV)-V characteristic. In *Photovoltaic Energy Conversion, Conference Record of the 2006 IEEE 4th World Conference on* (Vol. 2, pp. 2442-2445). IEEE.

[17] Dhimish, M., Holmes, V., Mehrdadi, B., Dales, M., Chong, B., & Zhang, L. (2017). Seven indicators variations for multiple PV array configurations under partial shading and faulty PV conditions. *Renewable Energy*.

[18] Lappalainen, K., & Valkealahti, S. (2017). Output power variation of different PV array configurations during irradiance transitions caused by moving clouds. *Applied Energy*, *190*, 902-910.

[19] Saidan, M., Albaali, A. G., Alasis, E., & Kaldellis, J. K. (2016). Experimental study on the effect of dust deposition on solar photovoltaic panels in desert environment. *Renewable Energy*, *92*, 499-505.

[20] Ramli, M. A., Prasetyono, E., Wicaksana, R. W., Windarko, N. A., Sedraoui, K., & Al-Turki, Y. A. (2016). On the investigation of photovoltaic output power reduction due to dust accumulation and weather conditions. *Renewable Energy*, *99*, 836-844.

[21] Dhimish, M., Holmes, V., Mehrdadi, B., & Dales, M. (2017). Diagnostic method for photovoltaic systems based on six layer detection algorithm. *Electric Power Systems Research*, *151*, 26-39.

[22] Dhimish, M., Holmes, V., Mehrdadi, B., & Dales, M. (2017). Multi-Layer Photovoltaic Fault Detection Algorithm. *High Voltage*.

[23] Roy, S. S., Mallik, A., Gulati, R., Obaidat, M. S., & Krishna, P. V. (2017, January). A Deep Learning Based Artificial Neural Network Approach for Intrusion Detection. In *International Conference on Mathematics and Computing* (pp. 44-53). Springer, Singapore.

[24] Kow, K. W., Wong, Y. W., Rajkumar, R. K., Rajkumar, R. K., & Isa, D. (2017). Incremental Unsupervised Learning Algorithm for Power Fluctuation Event Detection in PV Grid-Tied Systems. In *9th International Conference on Robotic, Vision, Signal Processing and Power Applications* (pp. 673-679). Springer Singapore.

[25] Mallor, F., León, T., De Boeck, L., Van Gulck, S., Meulders, M., & Van der Meerssche, B. (2017). A method for detecting malfunctions in PV solar panels based on electricity production monitoring. *Solar Energy*, *153*, 51-63.

[26] Li, Z., Wang, Y., Zhou, D., & Wu, C. (2012). An intelligent method for fault diagnosis in photovoltaic array. *System Simulation and Scientific Computing*, 10-16.

[27] Ducange, P., Fazzolari, M., Lazzerini, B., & Marcelloni, F. (2011, November). An intelligent system for detecting faults in photovoltaic fields. In *Intelligent systems design and applications (ISDA), 2011 11th international conference on* (pp. 1341-1346). IEEE.

[28] Bonsignore, L., Davarifar, M., Rabhi, A., Tina, G. M., & Elhajjaji, A. (2014). Neuro-fuzzy fault detection method for photovoltaic systems. *Energy Procedia*, *62*, 431-441.

[29] Dhimish, M., Holmes, V., Dales, M., Mather, P., Sibley, M., Chong, B., & Zhang, L. (2017, June). Fault detection algorithm for multiple GCPV array configurations. In *PowerTech, 2017 IEEE Manchester* (pp. 1-6). IEEE.

Appendix A:

1. If (PVD is 0-FaultyBypassDiode) and (POCV is 0-FaultyBypassDiode) then (Output is 1) (1)

2. If (PVD is 1-FaultyBypassDiode) and (POCV is 1-FaultyBypassDiode) then (Output is 2) (1)

3. If (PVD is 2-FaultyBypassDiodes) and (POCV is 2-FaultyBypassDiodes) then (Output is 3) (1)

4. If (PVD is 3-FaultyBypassDiodes) and (PSCC is 0-10%PartialShading) then (Output is 4) (1)

5. If (PVD is 3-FaultyBypassDiodes) and (PSCC is 10-20%PartialShading) then (Output is 5) (1)

6. If (PVD is 3-FaultyBypassDiodes) and (PSCC is 20-30%PartialShading) then (Output is 6) (1)

7. If (PVD is 3-FaultyBypassDiodes) and (PSCC is 30-40%PartialShading) then (Output is 7) (1)

8. If (PVD is 3-FaultyBypassDiodes) and (PSCC is 40-50%PartialShading) then (Output is 8) (1)

9. If (PVD is 3-FaultyBypassDiodes) and (PSCC is 50-60%PartialShading) then (Output is 9) (1)

10. If (PVD is 3-FaultyBypassDiodes) and (PSCC is 60-70%PartialShading) then (Output is 10) (1)

11. If (PVD is 3-FaultyBypassDiodes) and (PSCC is 70-80%PartialShading) then (Output is 11) (1)

12. If (PVD is 3-FaultyBypassDiodes) and (PSCC is 80-90%PartialShading) then (Output is 12) (1)

13. If (PVD is 3-FaultyBypassDiodes) and (PSCC is 90-100%PartialShading) then (Output is 13) (1)